How well does the Friends-of-Friends algorithm recover group properties from galaxy catalogues limited in both distance and luminosity?

Manuel Duarte, Gary A. Mamon

How well does the Friends-of-Friends algorithm recover group properties from galaxy catalogues limited in both distance and luminosity?

Manuel Duarte[*] and Gary A. Mamon

Institut d'Astrophysique de Paris, F-75014 Paris, France (UMR 7095: CNRS & UPMC)

ABSTRACT

The specific star formation rates of galaxies are influenced both by their mass and by their environment. Moreover, the mass function of groups and clusters serves as a powerful cosmological tool. It is thus important to quantify the accuracy to which group properties are extracted from redshift surveys. We test here the Friends-of-Friends (FoF) grouping algorithm, which depends on two linking lengths (LLs), plane-of-sky and line-of-sight (LOS), normalized to the mean nearest neighbour separation of field galaxies. We argue, on theoretical grounds, that LLs should be $b_\perp \simeq 0.11$, and $b_\parallel \approx 1.3$ to recover 95 per cent of all galaxies with projected radii within the virial radius r_{200} and 95 per cent of the galaxies along the LOS. We then predict that 80 to 90 per cent of the galaxies in FoF groups should lie within their parent real-space groups (RSGs), defined within their virial spheres. We test the FoF extraction for 16×16 pairs of LLs, using subsamples of galaxies, doubly complete in distance and luminosity, of a flux-limited mock Sloan Digital Sky Survey (SDSS) galaxy catalogue. We find that massive RSGs are more prone to fragmentation, while the fragments typically have low estimated mass, with typically 30 per cent of groups of low and intermediate estimated mass being fragments. Group merging rises drastically with estimated mass. For groups of three or more galaxies, galaxy completeness and reliability are both typically better than 80 per cent (after discarding the fragments). Estimated masses of extracted groups are biased low, by up to a factor 4 at low richness, while the inefficiency of mass estimation improves from 0.85 dex to 0.2 dex when moving from low to high multiplicity groups. The optimal LLs depend on the scientific goal for the group catalogue. We propose $b_\perp \simeq 0.07$, with $b_\parallel \simeq 1.1$ for studies of environmental effects, $b_\parallel \simeq 2.5$ for cosmographic studies and $b_\parallel \simeq 5$ for followups of individual groups.

Key words: methods: numerical – galaxies: clusters: general – galaxies: groups: general – dark matter.

1 INTRODUCTION

Galaxies are very rarely isolated: most live in pairs, groups and clusters of increasing richness and mass, with mean nearest neighbour separations only one or two orders of magnitude greater than their sizes (in contrast to stars within galaxies). The properties of galaxies are thus expected to be affected by their *global environment*, the mass of the group in which they reside, and by their *local environment*, the position they sit within their group. For example, their specific star formation rate (SSFR) is expected to be quenched by tidal stripping of their outer gaseous reservoirs by their group's gravitational potential (Larson, Tinsley & Caldwell 1980) and by ram pressure stripping of these reservoirs and possibly their interstellar gas by the intra-group gas (Gunn & Gott 1972). On the other hand, galaxy collisions and mergers should trigger bursts of star

formation (Joseph & Wright 1985), which should later deplete the galaxies of their gas for subsequent star formation. The respective roles of these physical processes are still unclear, hence it is important to probe the global and local environments of galaxies to which models of galaxy formation can be confronted.

Analyses of the effects of the group environment on the SSFR of galaxies have led to somewhat discrepant analyses. Peng et al. (2010) found that only galaxies of low stellar mass have their SSFR modulated by the environment, while von der Linden et al. (2010) find that the SSFR of high stellar mass galaxies are also somewhat modulated by their environment. The difference between these two studies is the lack of distinction between local and global environments by Peng et al.. But since it is notoriously difficult to properly define environment from redshift-space catalogues (Moore, Frenk & White 1993), one should strive towards optimal measures of galaxy groups.

Massive groups (i.e. clusters) are also useful as cosmological and physics tools. For example, the evolution of the cluster mass

[*] E-mail: duarte@iap.fr

function is a powerful diagnostic of cosmological parameters, including dark energy (Wang & Steinhardt 1998).

The extraction of group catalogues from redshift-space data is difficult for several reasons:

(i) It is intrinsically difficult to characterize systems of a few objects (galaxies).

(ii) The local environment requires an accurate definition of the group centre,[1] which is also difficult for low-multiplicity systems.

(iii) The Hubble flow creates redshift distortions (Jackson 1972) that cause galaxies within their virial spheres in real space to extend in redshift space by $\kappa \eta \sqrt{\Delta/2} \simeq 10$–20 virial radii along the line of sight (LOS), where $\kappa \simeq 2$–3 is the number of group velocity dispersions that one is studying, $\eta = \sigma_v/v_v \simeq 0.65$ (Mauduit & Mamon 2007; Mamon, Biviano & Boué 2013) is the group velocity dispersion in units of the circular velocity at the virial radius, and $\Delta \simeq 100$–200 is the mean overdensity at the virial radius relative to the critical density of the Universe (see Eke et al. 2004; Mamon, Biviano & Murante 2010). Such elongated groups along the LOS risk being confused with other foreground or background groups along the same LOS, situated with ±10–20 virial radii, i.e. typically 10–20 Mpc. In other words, different groups in real space risk being merged, while galaxies found in a group in redshift space may not lie within the virial sphere of that group in real space, leading to unreliable galaxy membership.

The most popular, and perhaps simplest algorithm is the *Friends-of-Friends* (FoF) percolation method, which, as implied by its name, puts into a single group all galaxies linked in pairs according to their separations along the LOS or on the plane-of-sky (POS).

Grouping algorithms are not limited to the FoF technique. Marinoni et al. (2002) have added Delaunay triangulation to Voronoi percolation. Moreover, several Bayesian methods have been recently developed, taking into account our *a priori*s, such as assuming NFW models (Navarro, Frenk & White 1996) for the number and mass density profiles of groups, to conform with the density profiles measured in Λcold dark matter (ΛCDM) haloes (Navarro et al. 1996). For example, Yang et al. (2005, 2007) used an iterative method to select groups, computing a density enhancement to assign galaxies to groups, starting with seed groups obtained from the FoF implementation of Eke et al. (2004). Muñoz-Cuartas & Müller (2012) also used an iterative method that can be compared to a FoF on dark matter haloes, starting with the assumption that all galaxies are their own halo (i.e. all groups have a single galaxy in the initial step). Domínguez Romero, García Lambas & Muriel (2012) also started with galaxies being alone in their groups, and adapted the Yang et al. (2007) algorithm by not directly assigning galaxies to groups, but computing instead probabilities that galaxies are in a given group, allowing galaxies during the iterative process to 'move' between groups; but they assigned galaxies to groups after the convergence of their iterative method. Finally, in Duarte & Mamon (in preparation), we have developed MAGGIE (Models and Algorithm for Galaxy Groups, Interlopers and Environment), another Bayesian and fully probabilistic grouping algorithm, which does not make use of the FoF technique.

Nevertheless, the FoF algorithm is still widely used, because the aforementioned Bayesian algorithms are not publicly available and are quite difficult to code on one's own. Moreover, the FoF algorithm has the advantage of providing unique group catalogues (in some other methods, the group catalogue depends on the galaxy one starts with), and makes no assumption on the properties of groups (i.e. number density profile or three-dimensional shape).

Many catalogues of galaxy groups have been constructed from redshift-space catalogues,[2] using FoF algorithms (Huchra & Geller 1982; Nolthenius & White 1987; Ramella, Geller & Huchra 1989; Trasarti-Battistoni 1998; Merchán & Zandivarez 2002; Eke et al. 2004; Berlind et al. 2006; Tago et al. 2010; Robotham et al. 2011; Tempel et al. 2014). Because of the redshift distortions, the physical linking lengths (LLs) are chosen to be of the order of 10 times longer for the LOS separations than for the POS ones. Moreover, for flux-limited galaxy catalogues, the physical LLs are scaled with the mean three-dimensional separation between neighbouring galaxies, $s \simeq n^{-1/3}$, where n is the mean number density of galaxies in the Universe at a given redshift (Huchra & Geller 1982). In other words, the FoF algorithm involves two dimensionless LLs :

$$b_\perp = \frac{\text{Max}(S_\perp)}{s}, \tag{1}$$

$$b_\parallel = \frac{\text{Max}(S_\parallel)}{s}, \tag{2}$$

where $S_\perp$ and $S_\parallel$ are the POS and LOS nearest neighbour separations, respectively.

Starting with Nolthenius & White (1987), nearly all FoF group analyses on redshift-space catalogues were accompanied with tests on mock galaxy catalogues derived from *N*-body simulations. However, not all FoF developers have applied the same tests to calibrate their LLs. Nolthenius & White (1987) were the first to compute the accuracy of group masses, as well as radii and velocity dispersions, crossing times and mass-to-light ratios. Ramella et al. (1989) were the first to test the recovered group multiplicity function. Frederic (1995) was the first to measure the galaxy reliability of extracted groups (comparing the FoFs of Huchra & Geller 1982 and Nolthenius & White 1987), as later done by Merchán & Zandivarez (2002), who also measured group completeness (against mergers of true groups) and reliability (against fragmentation of true groups). Eke et al. (2004) also tested the true group completeness and fragmentation, as well as the accuracy on group sizes and velocity dispersions. They also considered a quality criterion that amounts to a combination of galaxy completeness and reliability. Robotham et al. (2011) also considered a combination of fairly complex measures of group and galaxy completeness and reliabilities. Berlind et al. (2006) performed similar tests as Eke et al., with another test combining galaxy completeness and reliability. Berlind et al. noted that one cannot simultaneously optimize the accuracies on group sizes, velocity dispersions and [multiplicity function OR combined galaxy completeness/reliability].

Unfortunately, none of these studies is fully convincing: many did not perform the full suite of important tests, which we believe are true group fragmentation (group reliability) and merging (group completeness), galaxy completeness and reliability studied separately, and mass accuracy. Many have not measured the qualities of their LLs in terms of group parameters such as estimated mass and richness. Few studies have *optimized* the LLs: Eke et al. (2004) separately optimized $b_\perp$ and $b_\parallel$. Berlind et al. (2006) jointly optimized $b_\perp$ and $b_\parallel$ on a grid, for groups of 10 or more galaxies, while Robotham et al. (2011) jointly fit the LLs and their variation with density contrast and galaxy luminosity for groups of five or

---

[1] The group centre is also essential in all studies where groups are stacked.

[2] Turner & Gott (1976) applied a grouping algorithm in projected space that turned out to be a Friends-of-Friends algorithm.

Table 1. Friends-of-Friends LLs and physical parameters.

Authors	Sample	$b_\perp$	$b_\parallel$	$b_\parallel/b_\perp$	$\delta n/n$	κ
Huchra & Geller (1982)	CfA	0.23	1.34	6.3	20	5.7
Ramella et al. (1989)	CfA2	0.14	1.9	13	80	5.8
Trasarti-Battistoni (1998)	PPS2	0.13	1.7	13	108	4.9
Merchán & Zandivarez (2002)	2dFGRS	0.14	1.4	10	80	4.4
Eke et al. (2004)	2dFGRS	0.13	1.43	11	178	3.9
Berlind et al. (2006)	SDSS	0.14	0.75	5.4	86	2.3
Tago et al. (2010)	SDSS	0.075	0.75	10	565	1.7
Robotham et al. (2011)	GAMA	0.060	1.08	18	1100	2.2
Tempel et al. (2014) ($M_r < -19$)	SDSS	0.11	1.1	10	178	3.0
Tempel et al. (2014) ($M_r < -21$)	SDSS	0.066	0.67	10	830	1.4

Notes. The (normalized) LLs of Huchra & Geller (1982), Ramella et al. (1989), and Trasarti-Battistoni (1998) are derived (using equations 1 and 2) from their physical LLs at the fiducial distance and from the mean density at that distance, as derived by integrating the respective luminosity functions given by these authors. The LLs of Merchán & Zandivarez (2002) are estimated directly from the overdensity $\delta n/n$ given by these authors (using equation 3), those of Tago et al. (2010) are found from the densities deduced from the numbers of galaxies counted by these authors (again with equations 1 and 2). Eke et al. (2004) provide $b_\perp$ and $b_\parallel/b_\perp$, while Berlind et al. (2006) and Tempel et al. (2014) provide $b_\perp$ and $b_\parallel$. When not provided by the authors, the overdensity $\delta n/n$ is obtained through equation (3), and should be multiplied by 1.5 for a more accurate estimation (see text). Finally, the number of group velocity dispersions along the LOS, κ is obtained with equation (7) assuming $\Omega_m = 0.3$.

more galaxies. However, there is no strong agreement between the optimized LLs of Eke et al., Berlind et al., and Robotham et al. (see Table 1).

Moreover, we believe that in this era of large redshift surveys of $>10^5$ galaxies, it makes little sense to extract groups from flux-limited galaxy samples, for which most current implementations of the FoF algorithm scale the maximum separations proportionally to the separation between neighbouring field galaxies, $n^{-1/3}$. Indeed, since the minimum luminosity in flux-limited samples increases with redshift, the mean number density of galaxies decreases with redshift, and thus the mean separation between neighbouring galaxies increases with redshift. Therefore, the standard implementation of the FoF algorithm leads to groups that become increasingly sparse and with increasingly higher velocity dispersion with redshift (while their multiplicity function is preserved). Alternatively, since the mean neighbour galaxy separation increases with redshift in flux-limited samples, using a fixed physical LL leads to lower reliability at low redshift and lower completeness at higher redshifts. Moreover, grouping algorithms on flux-limited samples must evaluate the luminosity incompleteness as a function of redshift, which is difficult and imprecise (e.g. Marinoni et al. 2002; Yang et al. 2007). It is therefore much safer to consider subsamples that are complete in both distance and galaxy luminosity (as done for FoF grouping by Berlind et al. 2006, Tago et al. 2010 and Tempel et al. 2014). Admittedly, one recovers at best of order of one-quarter of the galaxies of the flux-limited sample, but one then avoids extracting a heterogeneous sample of groups (see Tempel et al. 2014) whose sizes and velocity dispersions stretch with redshift (when scaling the physical LLs with $n^{-1/3}$) or whose completeness and reliability vary with redshift (when adopting fixed physical LLs).

In the present work, we shall provide the first optimization of group LLs for doubly complete subsamples of galaxies, for six measures of the quality of the FoF grouping algorithm: minimal fragmentation and merging of true groups, maximum completeness and reliability of the galaxies of the extracted groups, and minimum

bias and inefficiency in the recovered group masses. These tests are performed on a wide grid of over 250 pairs of LLs. We have applied them to several doubly complete subsamples of galaxies cut from a mock flux-limited, Sloan Digital Sky Survey (SDSS)-like, sample of galaxies, and we analyse our results in terms of both true and estimated masses of the groups, as well as of their estimated richness.

We present the FoF algorithm in Section 2 and make predictions on its optimal parameters. In Section 3, we describe our mock real-space galaxy and group catalogues, and explain how we extract our mock redshift-space group catalogues. We define our tests in Section 4. In Section 5, we present the results of our tests, comparing to various grouping methods, and suggest an optimal set of LLs. Finally, we summarize and discuss our results in Section 6.

2 FRIENDS-OF-FRIENDS ALGORITHM

2.1 Predicted linking lengths and galaxy reliability

One can relate the choice of $b_\perp$ to the minimum galaxy overdensity (in number) of the groups with

$$\frac{\delta n}{n} = \frac{3}{4\pi b_\perp^3} - 1, \tag{3}$$

(from Huchra & Geller 1982). If galaxies are unbiased tracers of mass, i.e. $\delta n/n = \Delta/\Omega_m$, where Ω_m is the cosmological density parameter, then equation (3) easily leads to

$$b_\perp = \left(\frac{3/(4\pi)}{\Delta/\Omega_m + 1} \right)^{1/3}. \tag{4}$$

According to equation (4), if one desires to have virialized groups of overdensity (relative to critical) $\Delta = 200$, one requires $b_\perp \simeq 0.07$ (for $0.24 < \Omega_m < 0.35$). On the other hand, given $\Omega_m = 0.279$ or 0.317, respectively obtained with the 9th-year release of the *Wilkinson Microwave Anisotropy Probe* (Bennett et al. 2013) and the Planck mission (Planck Collaboration et al. 2013), one deduces $\delta n/n = 352$ and 326 from Bryan & Norman's (1998) approximation for Δ at the virial radius, leading to $b_\perp \simeq 0.09$ in both cases, according to equation (3).

One can also estimate the ratio of LOS to transverse LLs, as the ratio of LOS to POS group sizes caused by redshift distortions: if the LOS velocities span $\pm\kappa$ group velocity dispersions, the inferred LOS spread of distances in redshift space will be $\pm\eta\kappa\, v_{200}/H_0 = \pm\eta\kappa\sqrt{\Delta/2}\, r_{200}$ (see Mamon et al. 2010), where $\eta = \sigma_v/v_v \simeq 0.65$ for an NFW model with realistic concentration and velocity anisotropy (Mamon et al. 2013), and where we used equation (3). Therefore,

$$\frac{b_\parallel}{b_\perp} = \eta\,\kappa\,\sqrt{\frac{\Delta}{2}} \tag{5}$$

$$= \eta\,\kappa\,\sqrt{\frac{\Omega_m}{2}\left(\frac{\delta n}{n}\right)}. \tag{6}$$

Combining equations (4) and (5), one easily deduces

$$\kappa = \sqrt{\frac{8\pi}{3}}\,\eta^{-1}\,\Omega_m^{-1/2}\,\sqrt{b_\perp}\,b_\parallel. \tag{7}$$

For example, according to equation (5), probing galaxies along the LOS to $\pm 1.65\,\sigma_v$ (encompassing 95 per cent of the galaxies for Maxwellian LOS velocity distributions), for $\Delta = 200$, leads to $b_\parallel/b_\perp = 11$, hence with $b_\perp = 0.07$, one finds $b_\parallel = 0.7$ (the values are rounded off).

These theoretical LLs assume that groups are spherical and that all but one galaxy is in the centre. In fact, galaxies are distributed in a more continuous fashion (especially in rich groups and clusters). One can more accurately estimate the value of the transverse LL by writing

$$
\begin{aligned}
b_\perp &= \frac{\mathrm{Max}(S_\perp)}{n^{-1/3}}, \\
&= \frac{\mathrm{Max}(S_\perp)}{r_{\mathrm{vir}}} \frac{r_{\mathrm{vir}}}{n_{\mathrm{vir}}^{-1/3}} \left(1 + \frac{\delta n}{n}\right)^{-1/3}, \\
&= \left(\frac{3/(4\pi)}{\Delta/\Omega_{\mathrm{m}} + 1}\right)^{1/3} \frac{\mathrm{Max}(S_\perp)}{r_{\mathrm{vir}}} N_{\mathrm{vir}}^{1/3},
\end{aligned}
\tag{8}
$$

where one recognizes the previous estimate of $b_\perp$ (equation 4) in the first term of the right-hand side of equation (8).

We estimated the value of the second term of the right-hand side of equation (8) by running Monte Carlo simulations of cylindrical groups of unit virial radius with surface density profiles obeying the (projected) NFW model of scale radius of 0.2 (i.e. concentration 5). With 10 000 realizations each for $N = 2, 4, 8, 16, 32$ and 64 galaxies within the maximum projected radius allowed for the galaxies in the simulated groups, $R_{\mathrm{max}} = r_{200} = 1$, we found that the 95th percentile for the maximum — for all galaxies of the group — distance to the nearest neighbour is $\mathrm{Max}(S_\perp) \simeq 1.48 N^{-0.25}$ in units of the virial radius. Inserting this value of $\mathrm{Max}(S_\perp)/r_{\mathrm{vir}}$ into equation (8), with $\Delta = 200$ and $\Omega_{\mathrm{m}} = 0.25$, we predict that to obtain a completeness of 0.95, we require

$$
b_\perp \simeq 0.09 N^{0.08},
\tag{9}
$$

where we took into account that, for our adopted NFW model, the ratio of the number of galaxies within the virial sphere to that within the virial cylinder is $N_{\mathrm{vir}}/N \simeq 0.80$. Equation (9) predicts $b_\perp = 0.10$ for $N = 4$ and $b_\perp = 0.12$ for $N = 40$, i.e. $b_\parallel = 1.1$ for $N = 4$ and $b_\parallel = 1.3$ for $N = 40$, given $b_\parallel/b_\perp = 11$ found above. In other words, equation (3) underestimates $\delta n/n$ by a factor $\mathrm{Max}(S_\perp)/r_{\mathrm{vir}} N_{\mathrm{vir}}^{1/3} \simeq 1.4 N^{0.08}$, i.e. by 1.5 for $N = 4$ and 1.8 for $N = 40$. The slight increase of $b_\perp$ with richness suggests that fixing $b_\perp$ will lead to the fragmentation of rich groups.

Adopting instead the virial $\delta n/n = \Delta/\Omega_{\mathrm{m}} = 326$ (Planck, see above) would lead to $b_\perp = 0.14$ for $N = 4$ and $b_\perp = 0.17$ for $N = 40$. Since, at constant Δ, $b_\perp \propto \Omega_{\mathrm{m}}^{1/3}$ (equation 4), moving from $\Omega_{\mathrm{m}} = 0.25$ to $\Omega_{\mathrm{m}} = 0.3$ (a compromise between WMAP and Planck), keeping $\Delta = 200$, yields $b_\perp = 0.11$ ($N = 4$) or 0.13 ($N = 40$). According to equation (5), $b_\parallel/b_\perp$ does not vary with Ω_{m} at fixed Δ, hence we now obtain $b_\parallel = 1.3$.

Had we taken a maximum projected radius that is much smaller than r_{200}, we would obtain a much smaller value for $b_\perp$. Indeed, our Monte Carlo simulations indicate that with R_{max} and scale radius both equal to $0.2 r_{200}$, we find $\mathrm{Max}(S_\perp) \simeq 1.85 N^{-0.33}$ in units of R_{max}, hence $\mathrm{Max}(S_\perp)/r_{200} \simeq 0.37 N^{-0.33}$. Inserting this ratio into equation (8), we now obtain $b_\perp = 0.023$, independent of N. Thus, to first order, $b_\perp$ scales with R_{max}/r_{200}. Turning the argument around, a low $b_\perp$ leads to selecting galaxies in groups with projected radii limited to a small fraction of the virial radius.

We can also predict the reliability of the galaxy membership in groups, as follows. The expected number of interlopers from the extracted group out to a LOS distance of $\pm b_\parallel n^{-1/3}$ is

$$
N_{\mathrm{int}} \approx 2 \frac{N}{200} \frac{b_\parallel}{b_\perp},
\tag{10}
$$

where we simply stretched the group by a factor of $b_\parallel/b_\perp$ along the LOS, and where N is the number of galaxies in the real-space group (RSG). For $b_\parallel/b_\perp = 11$, equation (10) yields $N_{\mathrm{int}} = 0.44$ for $N = 4$ and $N_{\mathrm{int}} = 4$ for $N = 40$. Thus, the fraction of interlopers should roughly be independent of the richness hence mass of the RSG. For $b_\perp \simeq 0.1$, corresponding to groups with overdensity 200 relative to critical sampled at 95 per cent completeness, and sampling the LOS with 95 per cent completeness (leading to $b_\parallel/b_\perp = 11$), one then expects $N_{\mathrm{int}}/N = 0.11$. One then infers a galaxy reliability of $R = (N/N_{\mathrm{int}})/[1 + (N/N_{\mathrm{int}})] = 90$ per cent.

Equation (10) assumes that the Universe is made of spherical groups that are truncated at their virial radii. In fact, galaxy clustering brings galaxies close to groups, in a fashion that the radial number density profile pursues a gradual decrease beyond the virial radius. For NFW models of concentration of 5, the projected number of galaxies within the virial radius is $1/0.80 = 1.25$ times the number within the virial sphere. Hence the numbers of interlopers to the virial sphere should satisfy $N_{\mathrm{int}}/N = 0.25$. Then, one expects a reliability of $R = (N/N_{\mathrm{int}})/[1 + (N/N_{\mathrm{int}})] = 80$ per cent.

2.2 Previous implementations

Table 1 lists the dimensionless LLs for the different group FoF analyses. The values of $\delta n/n$ and κ of different FoF analyses, inferred from their LLs according to equations (3) and (6), are listed in Table 1. One sees that five of the nine previous studies advocate $b_\perp = 0.13$ or 0.14, and two (Eke et al. 2004 and Tempel et al. 2014 for $M_r < -19$) have pairs of LLs close to our predicted values of $(b_\perp, b_\parallel) \approx (0.11, 1.3)$. The two greatest outliers are Huchra & Geller (1982), whose transverse LL appears too large and Robotham et al. (2011), both of whose LLs appear too small. We will check these conclusions in Sections 5 and 6 using our analysis of mock galaxy and group catalogues.

2.3 Practical implementation of the FoF algorithm

There are two issues that need to be optimally handled when writing an FoF algorithm: rapidly extracting the separations in redshift space and properly estimating the mean density.

We followed the Huchra & Geller (1982) algorithm, used in most FoF implementations. Huchra & Geller write that two galaxies with redshifts z_i and z_j and an angular separation in θ_{ij} are linked using criteria that amount to

$$
\left(\frac{c}{H_0}\right)(z_i + z_j) \sin\left(\frac{\theta_{ij}}{2}\right) \le b_\perp n^{-1/3},
\tag{11}
$$

$$
\left(\frac{c}{H_0}\right) |z_i - z_j| \le b_\parallel n^{-1/3}.
\tag{12}
$$

We generalized[3] equations (11) and (12) to[4]

$$
\frac{d_{\mathrm{comov}}(z_1) + d_{\mathrm{comov}}(z_2)}{2} \theta \le b_\perp n^{-1/3},
\tag{13}
$$

$$
|d_{\mathrm{comov}}(z_1) - d_{\mathrm{comov}}(z_2)| \le b_\parallel n^{-1/3}.
\tag{14}
$$

---

[3] The *comoving distance*, $d_{\mathrm{comov}}(z) = c \int dz/H(z)$, in equation (13) should really be the *proper motion distance* $d_{\mathrm{pm}}(z) = d_{\mathrm{lum}}(z)/(1 + z) = (1 + z) d_{\mathrm{ang}}(z)$, but for flat cosmologies, $d_{\mathrm{pm}}(z) = d_{\mathrm{comov}}(z)$.

[4] Equation (13) is similar to the relation used by Zandivarez et al. (2014), with the exception of a minor difference in projected sizes given angle.

Table 2. Doubly complete mock galaxy subsamples.

ID	M_r^{max}	$L_r^{min}/L*$	z_{max}	Number	n (Mpc^{-3})	$n^{-1/3}$ (Mpc)	Fraction split
1	-18.5	0.09	0.042	47158	0.0125	4.32	0.053
2	-19.0	0.14	0.053	72510	0.0099	4.66	0.061
3	-19.5	0.22	0.066	112629	0.0078	5.05	0.066
4	-20.0	0.36	0.082	166899	0.0058	5.56	0.074
5	-20.5	0.56	0.102	213546	0.0040	6.29	0.086
6	-21.0	0.90	0.126	245821	0.0025	7.40	0.099

Notes. Columns are: sample, maximum *r*-band absolute magnitude, minimum luminosity in units of L_* (adopting $M_* = -20.44 + 5 \log h$ in the SDSS *r* band from Blanton et al. 2003), maximum redshift, sample size, mean density *n*, proxy for the mean separation to the closest neighbour, $n^{-1/3}$, and the percentage of true groups that are flagged because they are split during the simulation box transformations. The minimum redshift of each subsample is $z = 0.01$.

Thus, Huchra & Geller (1982) (also Berlind et al. 2006) neglected cosmological effects. For our deepest mock SDSS catalogue, at $z = z_{max} = 0.125$ (Catalogue 6, see Table 2), $d_{comov}/(cz/H_0) = 0.97$. So, the formula $d = cz/H_0$ leads to slightly too large distances, hence to slightly too strict choices of angles and differences in redshifts.

One could argue that, since groups are virialized, one ought to use the cosmological *angular distance*, $d_{ang}(z) = d_{comov}(z)/(1 + z)$ for the distances with which one computes the physical transverse separation in terms of the angular separation. But one should then also compress the LOS distances accordingly, and we are not aware of any work doing such a compression. Hence, we chose to stick with equations (13) and (14).

Since we are working with samples that are complete in luminosity, and since they are shallow enough that evolutionary effects are small, observers can estimate the mean number density of galaxies directly from the data.

Finally, for each galaxy, we computed the maximal angular distance to define the region in which potential neighbours could be found for the given transverse LL. With the celestial sphere grid that we have constructed (see Appendix A), we searched for galaxies obeying the criterion of equation (13), and then searched for galaxies meeting equation (14). The linked galaxies were then placed in a tree structure according to the Union-Find method (Tarjan & van Leeuwen 1984). Once all galaxies were analysed, we compressed the trees constructed with linked galaxies by replacing, in each group, the links of links with links to a single galaxy, giving us the identity of the group to which galaxies belong to. This implementation allows for a fast computation of galaxy groups for large samples of galaxies.

3 MOCK CATALOGUES

We wish to check if galaxy groups extracted with FoF algorithms are optimally selected. So our goal is to compare the *extracted groups* (EGs) in redshift space with the *true groups* (TGs) in real space. Since real space information is not directly accessible, we need to simulate it. The best way is to use mock galaxy catalogues constructed from the outputs of realistic galaxy simulations. These should include real space galaxy positions, comoving velocities, stellar masses and *r*-band luminosities, and the galaxies should be assembled in (real-space) groups with realistic density profiles and obeying the observed scaling relations. We then need to construct a redshift-space catalogue of groups from the real space catalogue of galaxies and groups.

3.1 Construction of mock real-space galaxy and group catalogues

There are two basic methods to build a mock catalogue of galaxies in real space.

(i) In the Halo Occupation Distribution method (Martínez & Saar 2002; Berlind & Weinberg 2002), the number of galaxies per halo is drawn from a probability distribution function that depends on the halo mass, or better, the galaxy luminosities or stellar masses are drawn from conditional luminosity (stellar mass) functions that depend on halo mass (Yang, Mo & van den Bosch 2003). The galaxy distribution is assumed to be spherically symmetric, and follows that of the dark matter particles in the haloes of ΛCDM cosmological simulations (e.g. NFW), the velocities are drawn from Maxwellian distributions (see Beraldo et al. 2014 for the limitations of this assumption), with radial and tangential velocity dispersions derived from the Jeans equation of local dynamical equilibrium, assuming some form for the radial variation of the velocity anisotropy.

(ii) In Semi-Analytical Models (SAMs; e.g. Roukema et al. 1997; Kauffmann et al. 1999), galaxy properties (in particular stellar mass and *r*-band luminosity) are painted on the haloes and subhaloes of cosmological *N*-body simulations across cosmic time, following well-defined recipes for star formation and galaxy feedback. This procedure produces galaxies that follow relatively well the observed properties and scaling relations.

We have chosen the second approach, because the recent SAM by Guo et al. (2011), run on the Millennium-II simulation (Boylan-Kolchin et al. 2009), fits well the $z = 0$ observations (as shown by Guo et al.). The Millennium-II simulation involved 2160^3 particles in a box of comoving size 137 Mpc, running with cosmological parameters $\Omega_m = 0.25$, $\Omega_\Lambda = 0.75$, $h = 0.73$, and $\sigma_8 = 0.9$. The particle mass was thus $9.5 \times 10^6\,M_\odot$.

We extracted the SAM output of Guo et al. (2011) from the Guo2010a data base on the German Astrophysical Virtual Observatory website.[5] The real-space TGs were extracted by Guo et al. using the FoF technique applied to the particle data, with over 10^5 particles for groups of mass $>10^{12}\,M_\odot$. The data base includes the mass within the sphere of radius r_{200}, where the mean mass density is $\Delta = 200$ times the critical density of the Universe, centred on the particle in Millennium-II simulation, within the largest subhalo, with the most negative gravitational potential (Boylan-Kolchin et al. 2009). We slightly modified the membership of the TGs by considering only the galaxies within r_{200}.[6]

3.2 Construction of mock redshift-space group catalogues

We now describe the construction of the mock SDSS redshift-space galaxy catalogue. We first note that our simulation box is not large enough to produce a deep enough redshift-space group catalogue. Indeed, the simulation box size limits the view to $z = 0.034$ from one corner to the next, or to $z = 0.058$ along the longest diagonal. We therefore replicated the simulation boxes along the three Cartesian coordinates to reach our desired maximum radius, thus creating a *superbox*. Moreover, since the SDSS survey is wider than $\pi/2$ sr (our mock SDSS has a solid angle of 2.2 sr), we could not place the observer at the corner of the superbox. Instead, we placed the

---

[5] http://gavo.mpa-garching.mpg.de/Millennium/Help, see Lemson & the Virgo Consortium (2006).

[6] We kept the galaxies outside the sphere of radius r_{200} as possible interlopers.
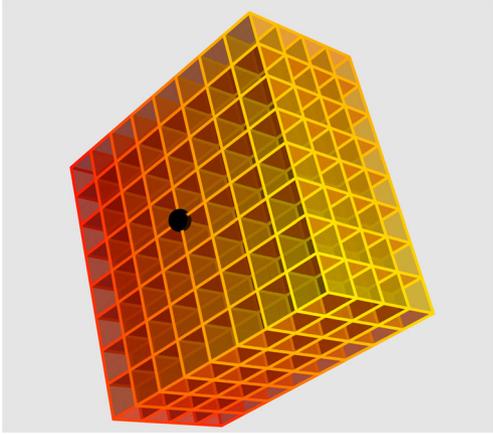
Figure 1. A representation of the full mock galaxy catalogue. Each small box is a 137 Mpc long cube. The observer is at the *large black point* in the middle of one of the square sides of the superbox.

observer at the middle of one of the sides of the superbox. Then, the size of the superbox must be double the proper distance of 505 Mpc to the highest redshift that we wish to sample, $z = 0.126$ (Table 2), along two directions, and 505 Mpc in the third (LOS) direction. One thus requires replicating the simulation cubes for a total of $4 \times 8 \times 8 = 256$ simulation cubes in our superbox (see Fig. 1). Because the redshifts are small, we only made use of the $z = 0$ simulation box, thus neglecting the small late evolution of group properties.

As pointed by Blaizot et al. (2005), this procedure of replicating can cause structures to appear periodically along the LOS. To avoid this feature, we followed Blaizot et al., applying random transformations on the boxes: $\pm \pi/2$ rotations around the three Cartesian axes, random periodic translations and random mirror reflections along a given axis. These transformations were applied to the phase space coordinates of galaxies.

We derived the coordinates of the galaxies on the sky, using standard formulae of spherical trigonometry. Absolute magnitudes were converted to apparent magnitudes, and the flux limit of the primary spectroscopic sample of the SDSS, $r < 17.77$, was applied. We assumed here that the observer knows how to correct his sample for Galactic and internal extinction, as well as k-correction, hence no backward corrections were applied to our mock galaxies.

From this flux-limited sample, we constructed subsamples that are doubly complete in distance and luminosity.[7]

We added the Hubble flow corresponding to the value of the Hubble constant used in the Millennium-II ($h = 0.73$). For this, we did not immediately compute LOS velocities. Instead, we derived the galaxy redshifts, z, by first solving for the redshift z_{cos} that a galaxy would have with zero peculiar velocity:

$$d_{comov}(z_{cos}) = d, \tag{15}$$

(where d is the Euclidean distance to the observer in the superbox) and then by determining the redshift given the galaxy's LOS peculiar velocity, $v_p^{LOS} = \boldsymbol{v}_p \cdot \boldsymbol{d}/d$, with (Harrison & Noonan 1979)

$$1 + z = \sqrt{\frac{1 + v_p^{LOS}/c}{1 - v_p^{LOS}/c}} \, (1 + z_{cos}) . \tag{16}$$

---

[7] This step of flux-limited sample can be avoided, but serves to show that our doubly complete subsamples are taken from the same parent sample.

We did not consider the SDSS limit on surface brightness, as it only affects a small fraction of the galaxies and surface brightness is not very well defined in the outputs of the SAM.

EG catalogues constructed as described above have two sets of unavoidable artefacts: 1. TGs that lie close the edges of the simulation box can be split during the process of random rotation, reflection and translation of the boxes. 2. Since the SDSS survey is not all-sky, TGs can be cut by the edges of the survey. We therefore first flagged the groups in real space that were split during the transformations (translations and rotations) of the simulation box. We neglected holes in our survey mask caused by spectroscopic incompleteness, bright stars, camera problems, etc., for technical simplicity. For example, the spectroscopic incompleteness is worse in regions of high surface density because of more frequent fibre collisions. Simulating this would require the calibration of incompleteness as a function of density in the SDSS sky and then apply it to our mock. This is complex and may not be accurate. Also, Berlind et al. (2006) found that fibre collisions only caused a small decrease (0.06 dex) of the group multiplicity function. Moreover, our goal is to test the FoF technique in a perfect situation, where all observational errors are neglected.

The resulting mock flux-limited catalogue, shown in Fig. 2, contains 823 497 galaxies.

3.3 Samples

Finally, we extracted several subsamples of galaxies and groups from our flux-limited sample, which are complete in both distance (volume) and luminosity (hereafter, *doubly complete*). We used half-integer values for the faintest absolute magnitude. We also adopted a minimum redshift of $z = 0.01$. Otherwise, at lower redshifts, peculiar motions of galaxies are non-negligible contributors to their redshifts, and thus contaminate the distances required to estimate the galaxy luminosities and stellar masses.

Our adopted doubly complete galaxy subsamples are listed in Table 2. Here, the mean density of each subsample is constant within, contrary to the flux-limited case. Subsample 1 spans deepest down the luminosity function to $0.09 L_*$, but has five times fewer galaxies than the two most distant samples. However, by only selecting galaxies more luminous than $0.9 L_*$, subsample 6 is limited to somewhat rare giant galaxies.

4 TESTING METHODS

We tested the FoF algorithm by running it on our mock redshift-space, doubly complete subsamples of galaxies, for a set of 16×16 geometrically spaced pairs of LLs. By directly comparing the properties of our EGs extracted in redshift space with their 'parent' TGs in real space, we could assess the performance of the FoF in recovering the real space information from the projected phase space observations. Note that TGs can have as little as one single member galaxy. Also, galaxies in redshift space with no linked galaxies can be considered as EGs with one single galaxy.

4.1 Linking real space and projected redshift space

There are several ways to link the EGs and TGs. We followed Yang et al. (2007), by linking the EG to the TG that contains the EG's most massive galaxy (MMG), and conversely linking the TG to the EG that contains the TG's MMG. With this definition for linking, we could easily associate FoF groups to real groups.
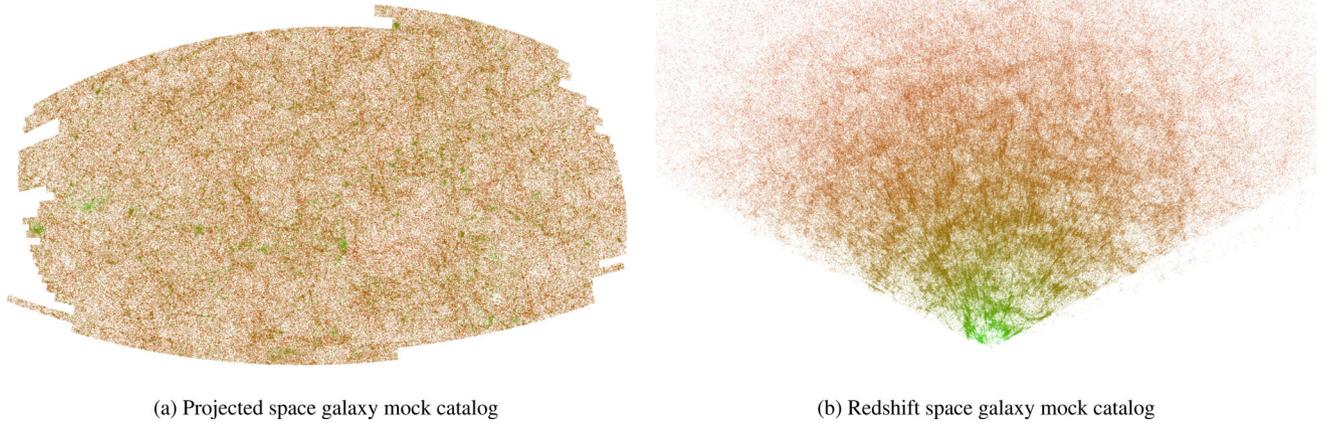
(a) Projected space galaxy mock catalog
(b) Redshift space galaxy mock catalog

Figure 2. Views of our initial, flux-limited, 2.2 sr SDSS mock galaxy catalogue, projection on the celestial sphere (left) and 3D cone (right, not sliced). The colours provide the absolute *r*-band magnitude (green for low luminosity). (a) Projected space galaxy mock catalogue. (b) Redshift-space galaxy mock catalogue.

4.2 Global tests

Our definition of the link between EGs and TGs allowed us to search for cases where there is no one-to-one correspondence between the groups in real and redshift space: a TG can suffer from *fragmentation* into several EGs, while an EG can be built from the *merging* of several TGs.

Fig. 3 illustrates different cases (following an analogous figure in Knobel et al. 2009). The top panel shows a one-to-one correspondence between the true and extracted groups.

We defined a fragmented TG as one that contains the MMGs of several EGs. Multiple situations can cause fragmentation of TGs. In some cases, the FoF algorithm fails to recover entire TGs, selecting instead its primary and secondary substructures (see panel, Fig. 3 b). In other cases, an EG is mostly composed of galaxies from one TG, but the MMG of another TG is 'accidentally' linked to the first TG. In consequence, the EG could be linked to a TG providing only a single member galaxy to the EG, in comparison with more members arising from another TG. When fragmentation occurred, we distinguished the *primary EG*, as that whose MMG corresponds to the MMG of the parent TG, from the other EGs, which we called *fragments*.

The dual of fragmentation is merging. In this situation, an EG contains the MMGs of several TGs. Proceeding similarly as for the case of fragmentation, we denoted *primary TG* of a given EG the TG whose MMG corresponds to the MMG of that EG, denoting the other TGs as *secondary*. An example of merging is shown in Fig. 3(c). Note that a true group can be fragmented and its primary extracted group can be the result of a merger of the true group with another one, as illustrated in Fig. 3(d).

4.3 Local tests

Our local tests check the membership of the EGs. We defined *completeness* as the fraction of galaxies in the TG (i.e. within the sphere of radius r_{200}) that were members of the primary EG. Given this definition, it did not make sense to consider the completeness for secondary fragments, hence we limited our tests to the primary EGs.

We defined *reliability* as the fraction of galaxies in the EG that were members of the parent TG (i.e. within the sphere of radius r_{200}). Here, we also limited our tests to the primary EGs.

Mathematically speaking, these definitions of galaxy completeness, C, and reliability, R, can respectively be written as

$$C = \frac{\text{TG} \cap \text{EG}}{\text{TG}},$$

$$R = \frac{\text{TG} \cap \text{EG}}{\text{EG}}.$$

Looking at Fig. 3, the completeness is the fraction of galaxies in the TG (left, green circles) recovered in the EG (right, red circles), while the reliability is the fraction of galaxies in the EG that belong to the TG.

These four quantities allow one to define the capacity of the FoF grouping algorithm (or any other grouping algorithm) to recover groups in real space from galaxy catalogues in redshift space.

Note that EGs that are fragments can have high reliability, while fragmentation causes primary EGs to have reduced completeness. When EGs are mergers of TGs, the secondary TGs lead to a decrease in the reliability, but can have high completeness.

4.4 Mass accuracy

There are many properties of groups that one wishes to recover with optimal accuracy (see Section 1). We focused here on one single property that appeared to us as the most relevant: the group total mass. We measured the masses of our EGs using the virial theorem formula of Heisler, Tremaine & Bahcall (1985)

$$M_{\text{EG}} = \frac{3\pi}{G} \langle R \rangle_{\text{h}} \sigma_v^2 = \frac{3\pi \, N}{2 \, G} \frac{\sum v_i^2}{\sum_{i<j} 1/R_{ij}}, \qquad (17)$$

where $\langle R \rangle_{\text{h}} = \langle 1/R_{ij} \rangle^{-1}$ is the harmonic mean projected separation, while σ_v is the unbiased measure of the standard deviation of the group velocities, given as solutions of equation (16) for $v_{\text{p}}^{\text{LOS}}$, replacing z_{cos} by the redshift of the MMG of the EG.

More precisely, we computed the accuracy of the log masses, respectively defining the *bias* and *inefficiency* as the median and equivalent standard deviation (half 16–84 interpercentile) of
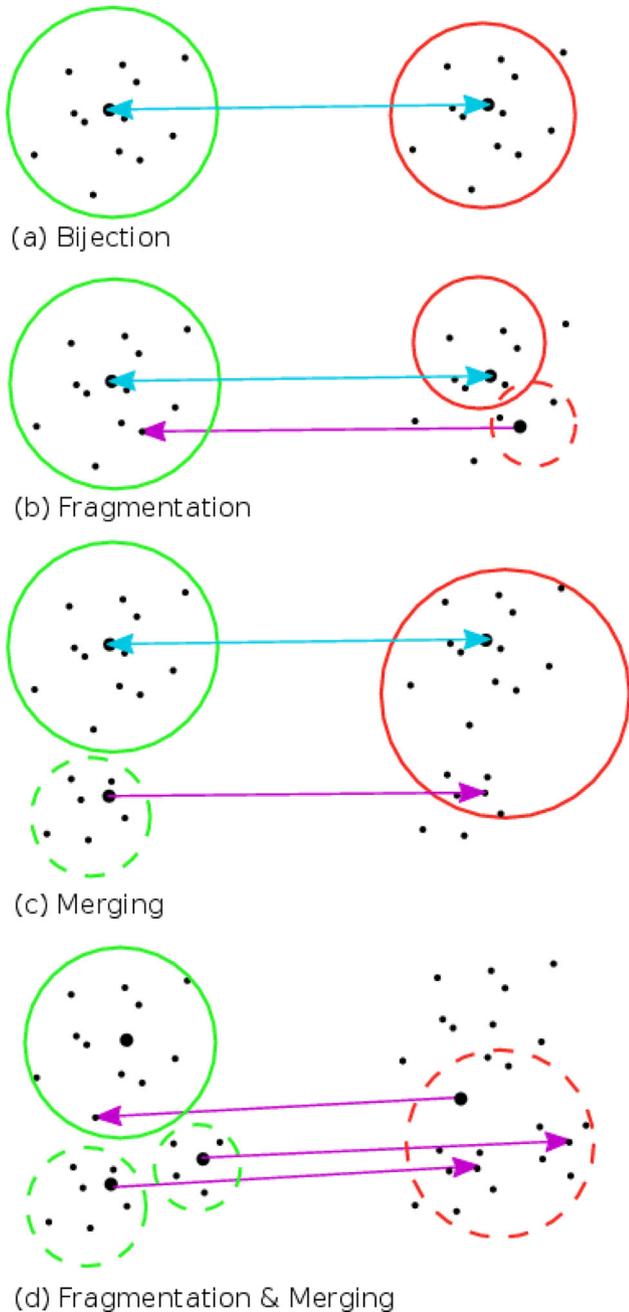
Figure 3. Schematic links between true groups (green circles) and FoF-extracted groups, (red circles), each with their respective MMG (black dots). The solid circles represent primary true and FoF groups, while the dashed circles respectively correspond to secondary true groups and FoF fragments. The cyan double arrows each indicate the one-to-one correspondence between the MMG in the true and extracted groups. The purple rightwards-pointing arrows correspond to the MMG of a true group ending up as a galaxy that is not the most massive of its extracted group. The purple leftwards-pointing arrows represent the cases where the MMG of an extracted group is not the most massive of its parent true group.

$\log(M_{EG}/M_{TG})$, where M_{TG} is the mass of the TG within the sphere of radius r_{200} (see Section 4.3).

4.5 Quality

It is not simple to extract a unique pair of optimal LLs from the four tests (fragmentation, merging, completeness, and reliability).

To reduce the number of tests, we combined fragmentation and merging into a single *global quality* and combined completeness and reliability into a single *local quality*.

We could define our qualities by multiplying F (fragmentation) by M (merging) and similarly, C by R. However, one could alternatively multiply $1 - F$ by $1 - M$, etc. Instead, we chose quality estimates that minimize the distance to the perfect case. The advantage of using distance rather than multiplying probabilities is that the former gives less weight to situations where one of the two parameters is perfect and not the other. For example, consider the case $F = M = p$. With the multiplication method, we would find that $Q = p^2$ is also reached with $F = \epsilon \ll 1$, yielding $M_{mult} = p^2/\epsilon$, which can be quite large (hence plenty of merging). On the other hand, with the distance method, we would find that $Q = p\sqrt{2}$ is also reached with $F = \epsilon \ll 1$ for $M_{dist} \simeq p\sqrt{2}$, which is much more restrictive. In a perfect algorithm, fragmentation and merging do not occur, hence $F = M = 0$, they are null. We therefore chose to minimize the *global quality*, defined as

$$Q_{global} = \sqrt{F^2 + M^2}. \tag{18}$$

Moreover, in a perfect grouping algorithm, the EGs are fully complete and reliable, i.e. $\langle C \rangle = \langle R \rangle = 1$, where the means are over all the groups of a mass bin. We, hereafter, drop the brackets, so that C and R should now be understood as means over groups within mass bins. We then define the *local quality* as

$$Q_{local} = \sqrt{(1 - C)^2 + (1 - R)^2}. \tag{19}$$

Both global and local qualities tend to zero for a perfect galaxy group algorithm. So the optimal LLs will be those that minimize Q_{global}, Q_{local}, mass bias and mass inefficiency. The maximum possible value of both qualities is $\sqrt{2}$.

4.6 Scope of the tests

We limit our tests to TGs containing at least three galaxies and that are not split by the transformations of the simulation box (see Section 3.2). Moreover, we only consider EGs with at least three galaxies and that do not lie near the survey edges (the virial radius, 2.3 Mpc, of a true group of log mass 15.2 in solar units, placed at $z = z_{min} = 0.01$, i.e. at an angle of more than 3°27) or redshift limits ($1.8\,v_{200} \approx 2.7\,\sigma_v$, of the same mass group, corresponding to $3073\,km\,s^{-1}$). Typically, 60 per cent (sample 2) to 25 per cent (sample 6) of the groups are flagged (see Appendix B). Finally, the tests of galaxy completeness and reliability, as well as mass bias and inefficiency, are restricted to primary EGs of TGs (not fragments).

5 RESULTS

We have applied the FoF algorithm on near and distant doubly complete subsamples (numbers 2 and 6 in Table 2), repeating the tests for a grid of 16×16 geometrically spaced pairs of LLs. The results of our tests are shown in Figs 4–10. The LLs of the different grouping studies listed in Table 1 are shown, except for Merchán & Zandivarez (2002), whose LLs nearly overlap with those of Eke et al. (2004).

5.1 Group fragmentation and merging

Fig. 4 indicates that, for the nearby doubly complete subsample (number 2), fragmentation only affects the massive TGs (up to ≈ 80 per cent of them for popular LLs), while Fig. 5 shows that,
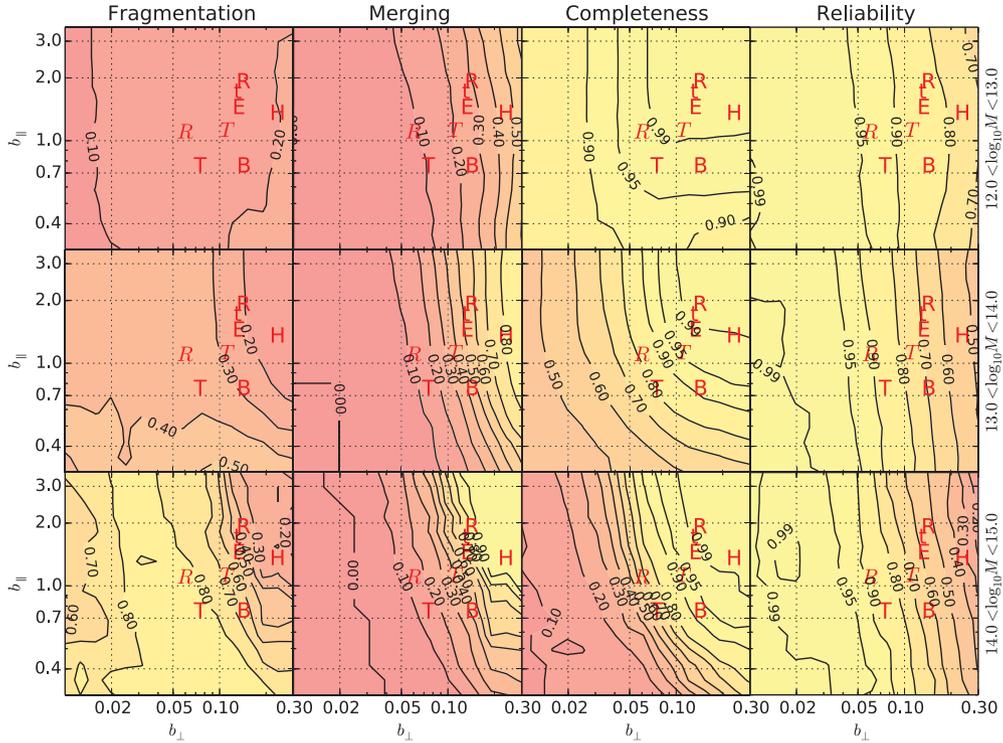
Figure 4. Contours of group fragmentation (first column) and merging (second column), as well as mean galaxy completeness (third column) and reliability (fourth column) computed for a 16×16 grid of LLs for the nearby doubly complete galaxy subsample 2 in Table 2. Results are shown for three bins of true group masses, for unflagged groups of at least three members (for both the extracted and parent groups), and further restricted to primary groups in the completeness and reliability panels. Pairs of LLs corresponding to previous are also shown as red letters (H: Huchra & Geller 1982; R: Ramella et al. 1989; t: Trasarti-Battistoni 1998; E: Eke et al. 2004; B: Berlind et al. 2006; T: Tago et al. 2010; *R*: Robotham et al. 2011; *T*: Tempel et al. 2014).
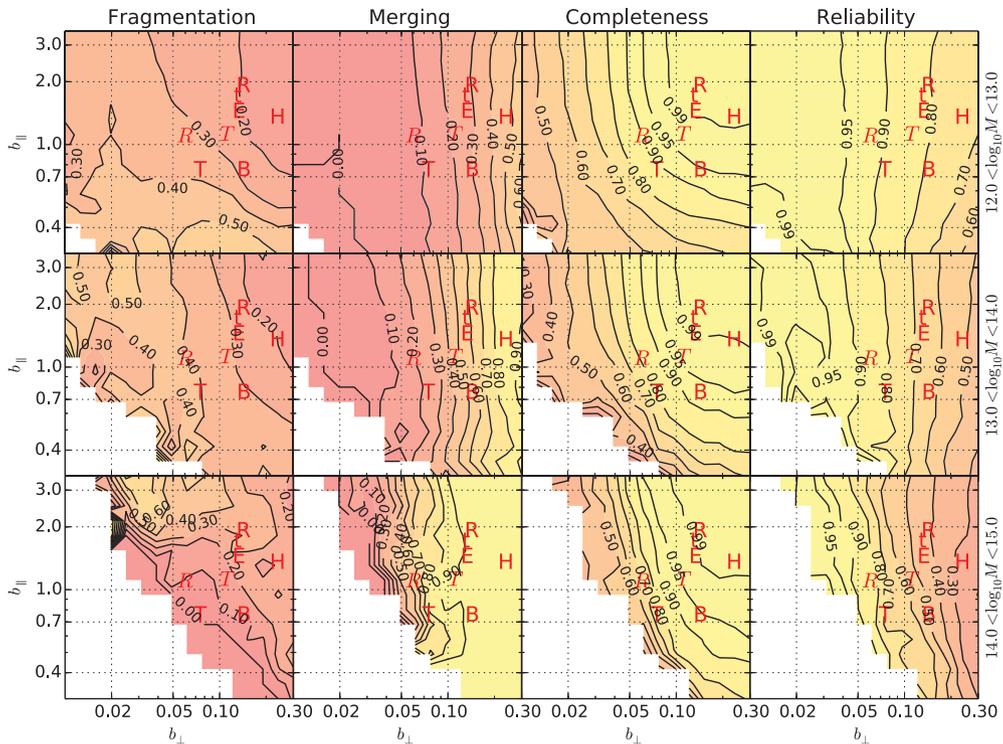
Figure 5. Same as Fig. 4, but where the different rows correspond to different bins of extracted group masses estimated from the virial theorem. The white zones show cases where the LLs led to no unflagged groups extracted.
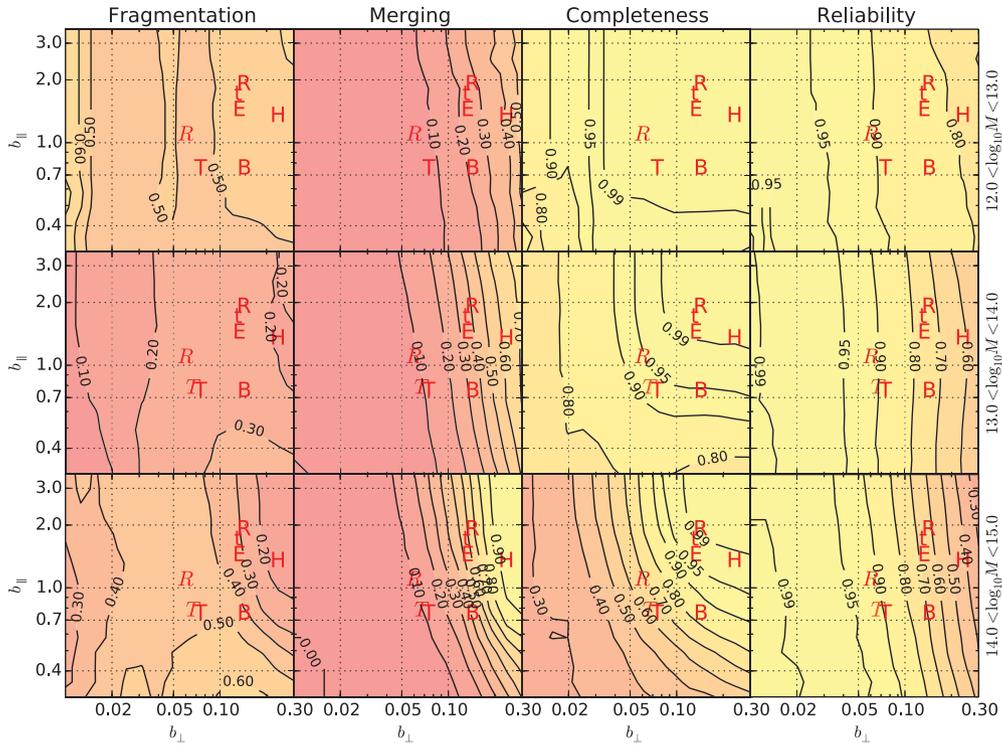
Figure 6. Same as Fig. 4, but for the distant doubly complete galaxy subsample 6 in Table 2.
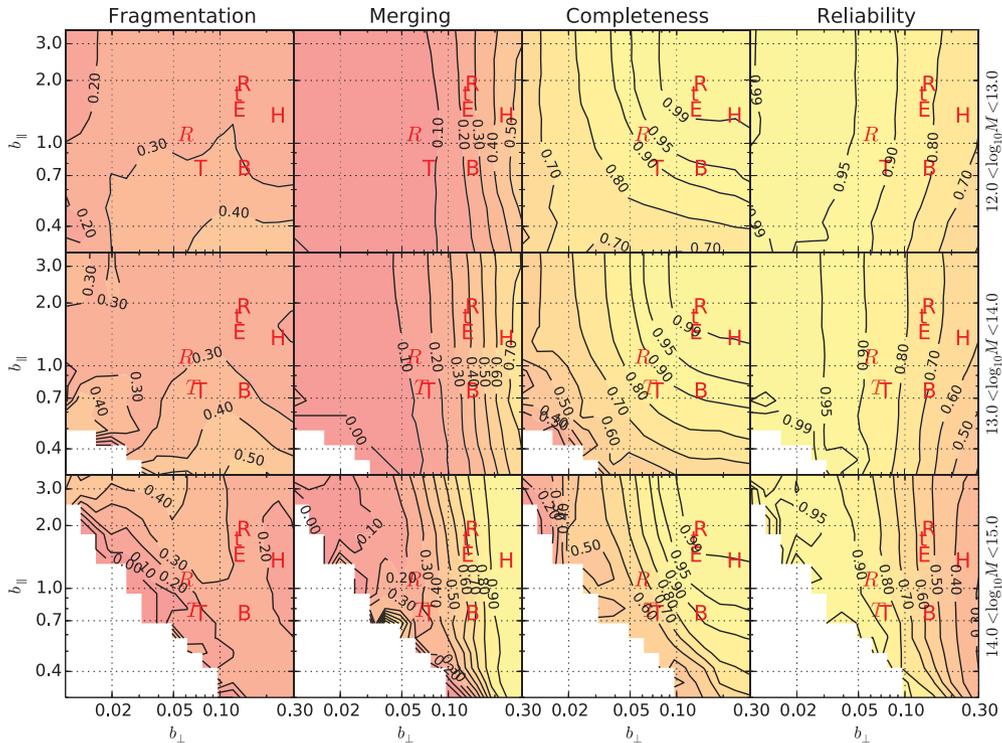

Figure 7. Same as Fig. 6, but where the different rows correspond to different bins of estimated masses.

for popular LLs, the fragmentation is lower (10–30 per cent) at high EG mass, hence fragment masses tend to be small (typically 20–40 per cent fragmentation at small and intermediate estimated masses).

On the other hand, the distant doubly complete subsample behaves in almost the opposite manner: fragmentation is most impor-

tant at the lowest TG masses (roughly 50 per cent fragmentation, Fig. 6) and is independent of estimated EG masses (at roughly 20–30 per cent; Fig. 7).

In any event, fragmentation tends to decrease with greater LLs, as expected, although it decreases somewhat faster with increasing $b_\perp$ than with increasing $b_\parallel$.
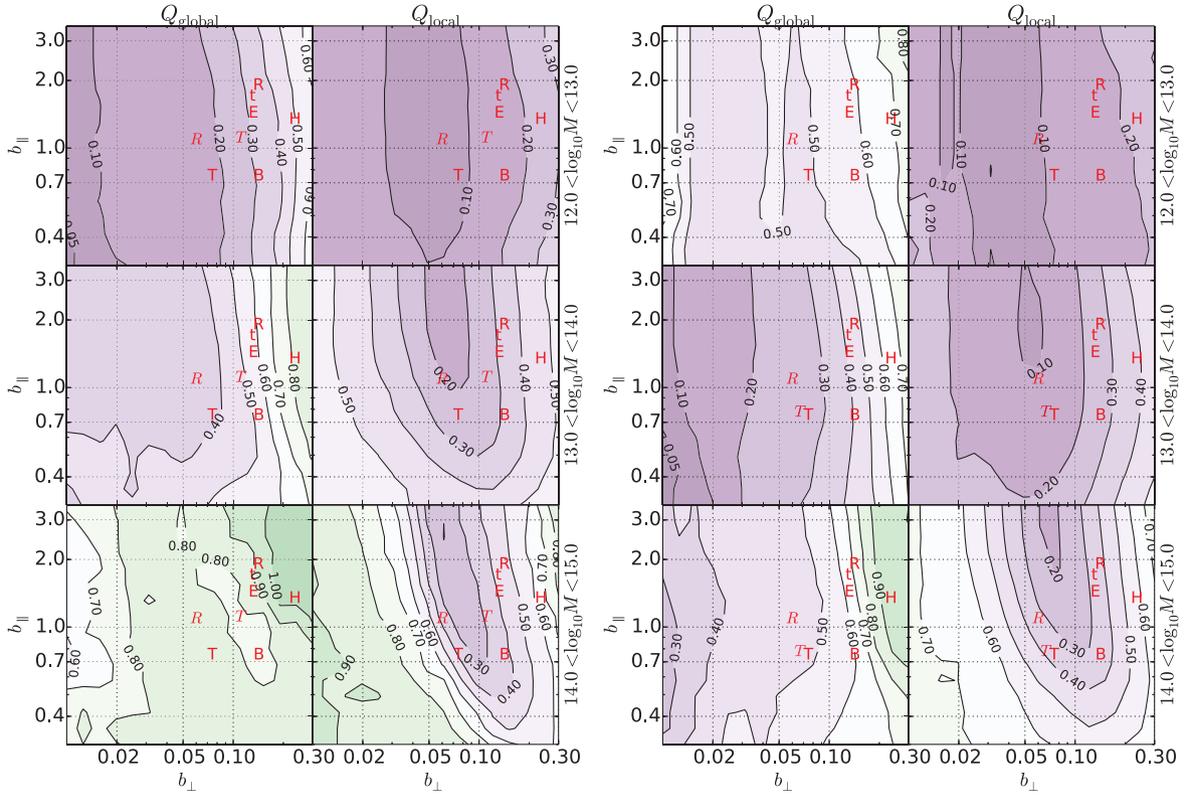
Figure 8. Global and local quality factors in a 16×16 grid of LLs for subsamples 2 (left) and 6 (right), in three bins of true masses. Results are shown for unflagged groups (restricted to primary groups for Q_{local}) of at least three members (in both the true and extracted group). The symbols are as in Fig. 4.
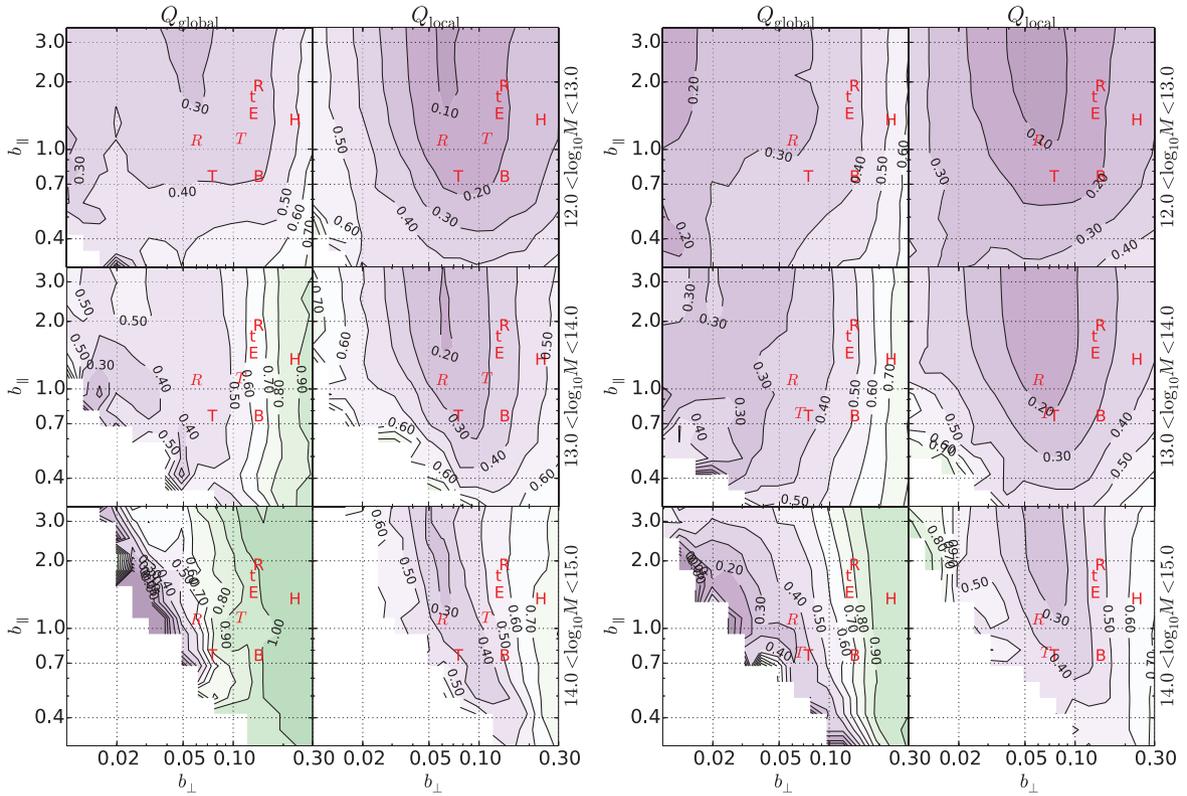

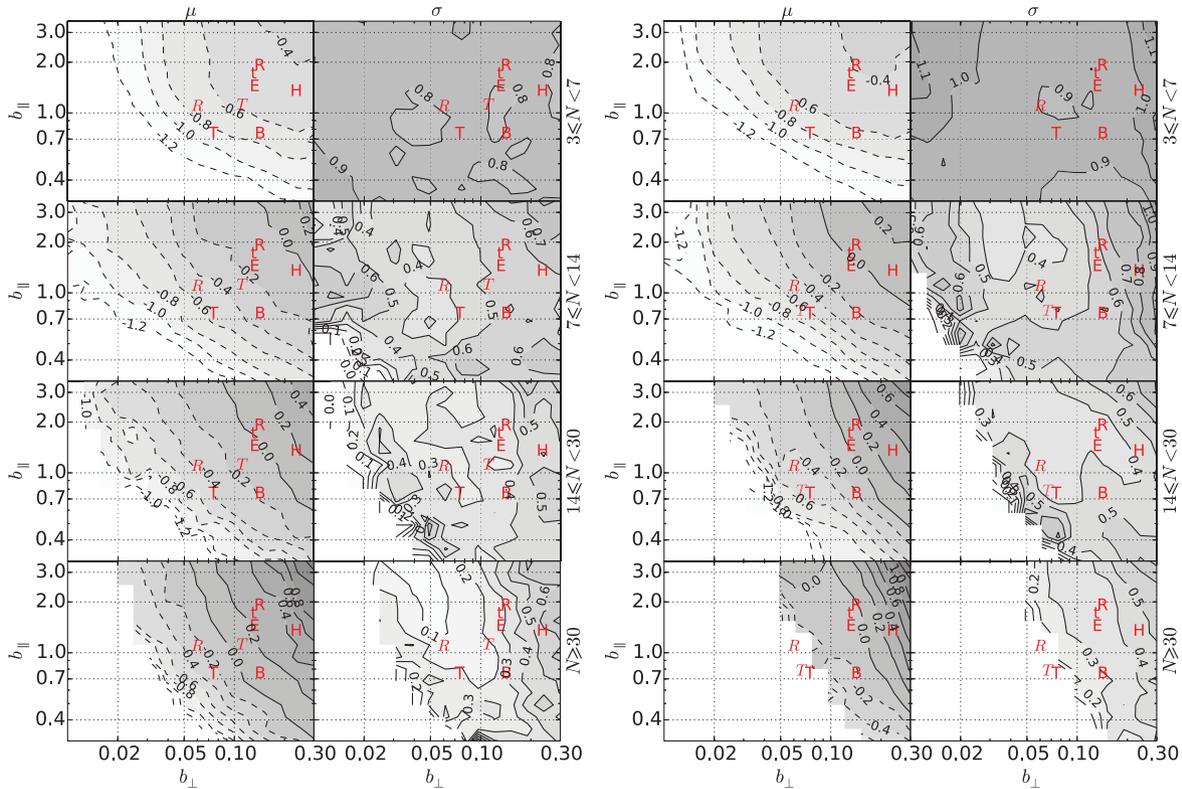**Figure 9.** Same as Fig. 8 but in bins of estimated masses. The white zones show cases where the LLs led to no unflagged groups extracted.

Figure 10. Bias (μ) and inefficiency (σ) of the group masses estimated by the virial theorem (equation 17) on our 16×16 grid of LLs, in four bins of extracted group richness (we do not consider extracted groups for which the parent true group has ≤ 3 members). The bias and inefficiency are respectively computed as the median and half 16–84 interpercentile of $\log_{10}(M_{EG}/M_{TG})$. Results are shown for primary, unflagged groups. The left and right panels are, respectively, for galaxy subsamples 2 and 6. The symbols are as in Fig. 4. The white zones indicate LLs with no unflagged groups extracted.

Since merging is the dual of the fragmentation, one expects the level of merging to vary in the opposite way as fragmentation. Indeed, Figs 5 and 7 indicate that merging becomes more important at higher estimated masses, respectively reaching up to 90 per cent and 65 per cent for high estimated masses with popular choices of LLs in subsamples numbers 2 and 6. However, Figs 4 and 6 show that the merging fraction increases only slowly with TG increasing mass, with typically 15–40 per cent (increasing fast with $b_\perp$) of the TGs being merged with other ones. Finally, merging decreases with smaller LLs, especially with smaller $b_\perp$.

Figs 8 and 9 show the Q_{global} quality indicator that combines fragmentation and merging into a single parameter. These figures show that decreasing $b_\perp$ leads to a better tradeoff between fragmentation and merging, i.e. that the decrease of merging with decreasing $b_\perp$ has a stronger effect than the increase of fragmentation with decreasing $b_\perp$: the optimal Q_{global} is often reached for $b_\perp < 0.02$.

5.2 Galaxy completeness and reliability

Figs 4 and 6 indicate that completeness is very high (>99 per cent) at low TG masses, and decreases to lower values ($60 - 99$ per cent) at high TG mass. A weaker trend occurs when EG mass is substituted for TG mass (see Figs 5 and 7). Since high-mass TGs are less complete, their estimated masses should be smaller, and the EGs with high masses will be the lucky complete ones, which explains the weaker trend of completeness with EG mass. Note that we are only considering primary groups of at least three members. The transverse and LOS LLs have roughly the same impact on galaxy completeness.

The reliability of the group membership decreases with increasing EG mass (Figs 5 and 7): regardless of the subsample, the reliability is 80–90 per cent for low-mass EGs, but only 50–85 per cent for high-mass EGs. The value of $b_\parallel$ has virtually no effect on galaxy reliability. We will discuss this lack of convergence of the reliability with $b_\parallel$ in Section 6.

Galaxy reliability also decreases with the masses of the TGs, but the trend is weaker (Figs 4 and 6): as the reliability decreases from 85–95 per cent to 60–90 per cent, roughly independent of the subsample.

The right panels of Figs 8 and 9 show that, again, the transverse LL appears to be more decisive than the LOS one when combining galaxy completeness and reliability into a single local quality factor.

5.3 Mass accuracy

The left columns of the two panels of Fig. 10 show that the primary EG masses recovered by the FoF algorithm are systematically biased low: for the popular choices of LLs, the bias (μ) is as strong as -0.6 ± 0.2 dex at low multiplicity ($3 \leq N_{EG} \leq 6$), decreasing to 0.0 ± 0.3 dex at high multiplicity ($N_{EG} \geq 30$).

The right columns of the two panels of Fig. 10 indicate that, even if the biases could be corrected for, the masses cannot be recovered to better than 0.8–0.9 dex at low multiplicity, improving to 0.2 dex at high multiplicity. The inefficiency (σ) is minimal for $b_\perp \approx 0.05$ (within a factor of 2) and $b_\parallel \approx 1.0$ (low richness) or $b_\parallel \gtrsim 1.0$ (intermediate and high richness). For transverse LLs within 40 per cent of $b_\perp = 0.1$, the inefficiency is not very insensitive to $b_\parallel$.

The situation becomes even worse when fragments are included in the statistics. In this work, we have separated the accuracy of the group masses with the occurrence of group fragmentation. But observers cannot tell if a group is a fragment or a primary EG.

6 CONCLUSIONS AND DISCUSSION

Before testing the FoF algorithm using a mock galaxy catalogue in redshift space, we first argued on physical grounds (Section 2.1) that the normalized transverse LL ought to be $b_\perp \approx 0.10$ (slightly increasing with richness) to extract 95 per cent of the galaxies within the virial radius of NFW true groups. We also argued that, restricting the galaxies along the LOS to $\pm 1.65\,\sigma_v$ (95 per cent of the galaxies) for groups defined to be 200 times denser than the critical density of the Universe requires $b_\parallel/b_\perp \approx 11$, hence $b_\parallel \simeq 1.1$. These LLs are estimated from our mocks that are based upon the Millennium-II simulation that had adopted $\Omega_m = 0.25$. Converting to $\Omega_m = 0.3$ yields $b_\perp = 0.11$ and $b_\parallel = 1.3$. Finally, estimating the contamination by interlopers, we predict between 80 per cent (NFW model extended outwards) to 90 per cent (NFW model truncated to sphere plus random interlopers) galaxy reliability.

We then built a mock redshift-space galaxy catalogue with the properties of the flux-limited SDSS primary spectroscopic sample, from which we extracted two subsamples that are doubly complete in distance and luminosity (Section 3). We extracted groups from both of these subsamples, running the standard FoF algorithm for 16×16 pairs of LLs. In each case, we measured the fraction of true groups that were fragmented in the FoF extraction process, the fraction of extracted groups that were built by the merging of several true groups, as well as the bias and inefficiency with which the group masses were extracted. Moreover, we computed the completeness and reliability of the galaxy membership relative to the spheres of radius r_{200} in which the true groups are defined.

We analysed group fragmentation, merging, galaxy completeness and reliability, mass bias and inefficiency for two doubly complete subsamples and in bins of true and estimated mass or estimated richness (for the mass accuracy).

We found that massive true groups are more prone to fragmentation, as expected, but that, for popular choices of LLs, the probability of fragmentation is greatest (30 per cent) at low estimated mass, i.e. the fragments are of low mass. The process of fragmentation of rich (massive) groups is similar to images of large galaxies being preferentially fragmented by automatic image extraction pipelines (e.g. De Propris et al. 2007).

Group merging is low at low estimated mass, but increases drastically to reach 40–90 per cent (for popular LLs) at high estimated mass. Galaxy completeness is high, typically >80 per cent. Galaxy reliability is typically 75 to 90 per cent depending on group mass.

Our analytical prediction of 95 per cent completeness for $b_\perp \simeq 0.10$ is only met for groups of high true masses (Figs 4 and 6). Groups of low mass will have more concentrated galaxy populations, which will lead to smaller values of $\mathrm{Max}(S_\perp)/r_{200}$, hence smaller values of $b_\perp$. Also, our analytical prediction of 80–90 per cent reliability for groups with $b_\perp = 0.10$, $b_\parallel = 1.1$ is accurate for groups of all masses of the distant subsample (Fig. 6). However, for the nearby subsample (2), our predicted reliabilities are only accurate for groups of low true masses, but optimistic for higher mass groups, for which $R \simeq 70$–75 per cent.

Group merging and galaxy reliability depend little on $b_\parallel$, especially at high transverse LL, $b_\perp > 0.1$, where the galaxies are extracted to projected radii beyond r_{200}, hence the contamination by interlopers is mainly in the transverse direction. This lack of
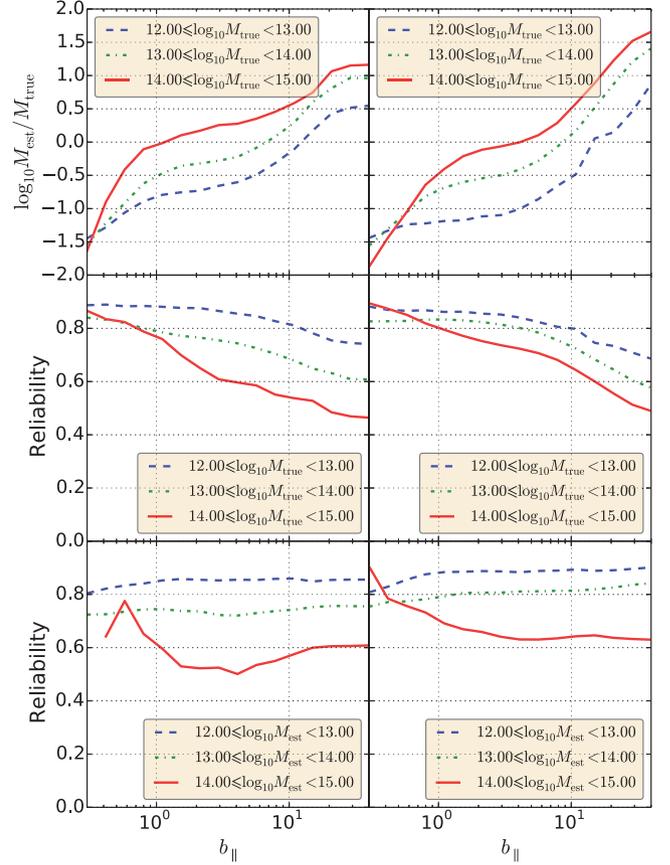

Figure 11. Variation of the mass bias and reliability as a function of $b_\parallel$ for $b_\perp = 0.1$, for subsamples 2 (left) and 6 (right).

optimal $b_\parallel$ for galaxy reliability may seem surprising at first. We checked our analysis by measuring the reliability for $b_\perp = 0.1$, for a very wide range of $b_\parallel$ extending from 0.3 to 40. The top panels of Fig. 11 indicate that the reliability does end up decreasing fairly fast beyond some large value of $b_\parallel \simeq 6$, i.e. beyond the limits of Figs 4 and 6. The second row of panels of Fig. 11 shows a different behaviour in bins of estimated mass. This is the consequence of the estimated mass increasing very fast with $b_\parallel$, as shown in the bottom panels of Fig. 11. The increase, with increasing $b_\parallel$, of the mass bias is qualitatively parallel to the corresponding decrease of the reliability (in bins of TG mass). At low $b_\parallel$, the reliability decreases fairly rapidly and the mass bias increases rapidly (towards zero), then both settle into an almost constant plateau in the range $1.4 \lesssim b_\parallel \lesssim 8$, then both worsen rapidly up to $b_\parallel \simeq 25$, beyond which both saturate, because the longitudinal link is so large that one reaches the minimum and maximum redshifts of the subsample, where most groups are flagged. Massive groups that are built from TG merging can be fairly reliable if the secondary TGs have negligible mass relative to the primary one. This explains why R remains fairly high when M is high. The plateau around $b_\parallel \approx 3$ appears to represent the range of optimal longitudinal LLs.

An illustration is given in Fig. 12, where a given EG has reached the limits of the catalogue with a very large value of $b_\parallel$. Fig. 12 also shows that interloping TGs are highly clustered. This may explain why increasing $b_\parallel$ has only a small effect on galaxy reliability: there is a void behind the main TG (black outer circles).

While fragmentation, measured in bins of true group mass, decreases with increasing $b_\parallel$, as expected (Figs 4 and 6), we find that
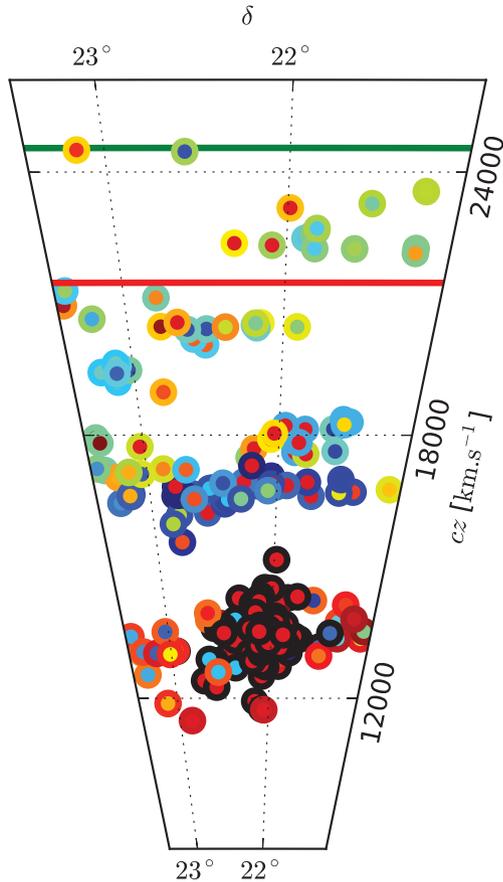
Figure 12. An example of group and halo for $b_\parallel = 20.8$ and $b_\perp = 0.1$ for subsample 4. The width of the cone is exaggerated by a factor of roughly 5 for illustrative purposes. Outer and inner circle colours respectively refer to the TGs and EGs. The horizontal green and red lines, respectively, indicate the maximum redshift, z_{max} and the redshift where galaxies are flagged for being close to z_{max}. Some galaxies of the red EG, whose TG is the black one, are flagged for being close to z_{max}, hence the group would not be considered in our tests.

in bins of estimated mass, the fraction of groups that are (secondary) fragments increases with $b_\parallel$ (Figs 5 and 7). We believe that this is caused by interlopers increasing the group estimated mass (Fig. 11).

The masses, estimated with the virial theorem (equation 17), are a strong function of the multiplicity of the extracted group. The estimated masses are systematically biased low, especially for low extracted group multiplicities (typically by a factor of 4!). Similar trends have been found for FoF groups (Robotham et al. 2011) and for other, mostly dynamical, group mass estimators (Old et al. 2014). The estimated group masses are inaccurate, even after correcting for the biases: the typically errors are 0.8–0.9 dex at low multiplicity, decreasing to 0.2 ± 0.1 dex at high multiplicity.

The optimal completeness and reliability of the galaxy membership lead to fairly extreme LLs, i.e. $b_\perp < 0.1$ and $b_\parallel > 2$. However, the use of such a small transverse LL amounts to extracting the inner regions of groups, thus missing their outer envelopes. Indeed, one notices that fragmentation worsens at increasingly lower values of $b_\perp$. Therefore, our attempt to define a local quality by combining galaxy completeness and reliability is of little use if one wishes to recover galaxies out to close to the virial radii of groups.

In fact, the optimal LLs depend on the scientific goal:

(i) statistical studies of environmental effects require high reliability (say $R > 0.9$), accurate masses and, to a lesser extent, minimal fragmentation.

(ii) cosmographical studies of group mass functions require accurate masses, minimal group merging and fragmentation.

(iii) studies for followups at non-optical wavelengths (e.g. X-rays) benefit from high completeness.

For statistical studies of environmental effects, it seems best to adopt $b_\perp \simeq 0.06$, $b_\parallel \approx 1.0$, for which the reliability is roughly as high as it gets for the choice of $b_\perp$: over 90 per cent at low M_{EG} and over 80 per cent at intermediate and high M_{EG}. Then, the completeness is higher than 70 per cent at high estimated mass and much higher at low M_{EG}. The mass inefficiency is minimal, but with this choice of LLs, there will be virtually no EGs with more than 30 galaxies in the distant more luminous subsample (Fig. 10).

This choice of LLs is close to that of Robotham et al. (2011), which may seem obvious since both studies used some form of optimization of the LLs. However, the details of the optimization criteria are somewhat different: Robotham et al. multiplied four criteria: basically the group completeness and reliability, which bears some resemblance to our group fragmentation and merging, but theirs is based on TG-EG pairs that have more than half their galaxies in common, as well as two measures of a combination of galaxy completeness and reliability, averaged over TGs and EGs, respectively. Our analysis differs in that we directly constrained group fragmentation and merging, as well as galaxy completeness and reliability for primary fragments, and finally mass accuracy.

For cosmographical and other studies involving accurate group mass functions, it appears best to adopt $b_\perp \simeq 0.05$, $b_\parallel \simeq 2$, as lower $b_\parallel$ increases fragmentation (Figs 5 and 7), while higher $b_\parallel$ causes too high group fragmentation at high EG masses. This value of $b_\parallel \simeq 2$ is in agreement with the intersection of the regions of $(b_\perp, b_\parallel)$ space that optimize both the multiplicity function and velocity dispersions obtained by Berlind et al. (2006).

Finally, for non-optical followups, for which galaxy completeness is perhaps the sole important parameter, one should privilege large LLs, e.g. $b_\perp \simeq 0.2$, $b_\parallel \simeq 2$–4. However, one can also adopt $b_\perp = 0.1$, $b_\parallel \simeq 2$–4, for which the completeness is greater than 95 per cent at all masses and for both subsamples.

Converting from $\Omega_m = 0.25$ (Millennium-II Simulation) to $\Omega_m = 0.3$ (WMAP-Planck compromise), $b_\perp$ must be increased by 6 per cent (equation 4) to $b_\perp \simeq 0.07$ for the choices optimizing environmental or cosmographical studies. Since $b_\parallel/b_\perp$ is independent of Ω_m at given Δ, $b_\parallel$ must also be increased by 6 per cent, i.e. to $b_\parallel \approx 1.1$ for environmental studies.

We finally note that while high estimated mass group fragmentation and merging depend on the particular doubly complete subsample, galaxy completeness and reliability as well as mass accuracy depend little on the subsample. Berlind et al. (2006) had similarly concluded that the doubly complete subsample influenced little their tests of the group multiplicity function and the accuracy of projected radii and velocity dispersions.

FoF grouping techniques can be used as a first guess for other more refined grouping methods (Yang et al. 2005, 2007). In a future paper (Duarte & Mamon, in preparation), we will present another grouping algorithm, which is not an FoF, but is instead a probabilistic grouping algorithm that is built upon our current knowledge of groups and clusters (partly from X-rays and independent of FoF analyses of optical galaxy samples) and from cosmological *N*-body simulations.

REFERENCES

Bennett C. L. et al., 2013, ApJS, 208, 20
Beraldo L. J., Mamon G. A., Duarte M., Peirani S., Boué G., 2014, MNRAS, preprint (arXiv:1310.6756)
Berlind A. A., Weinberg D. H., 2002, ApJ, 575, 587
Berlind A. A. et al., 2006, ApJS, 167, 1
Blaizot J., Wadadekar Y., Guiderdoni B., Colombi S. T., Bertin E., Bouchet F. R., Devriendt J. E. G., Hatton S., 2005, MNRAS, 360, 159
Blanton M. R. et al., 2003, ApJ, 592, 819
Boylan-Kolchin M., Springel V., White S. D. M., Jenkins A., Lemson G., 2009, MNRAS, 398, 1150
Bryan G. L., Norman M. L., 1998, ApJ, 495, 80
De Propris R., Conselice C. J., Liske J., Driver S. P., Patton D. R., Graham A. W., Allen P. D., 2007, ApJ, 666, 212
Domínguez Romero M. J. d. L., García Lambas D., Muriel H., 2012, MNRAS, 427, L6
Eke V. R. et al., 2004, MNRAS, 348, 866
Frederic J. J., 1995, ApJS, 97, 259
Gunn J. E., Gott J. R., 1972, ApJ, 176, 1
Guo Q. et al., 2011, MNRAS, 164
Harrison E. R., Noonan T. W., 1979, ApJ, 232, 18
Heisler J., Tremaine S., Bahcall J. N., 1985, ApJ, 298, 8
Huchra J. P., Geller M. J., 1982, ApJ, 257, 423
Jackson J. C., 1972, MNRAS, 156, 1P
Joseph R. D., Wright G. S., 1985, MNRAS, 214, 87
Kauffmann G., Colberg J. M., Diaferio A., White S. D. M., 1999, MNRAS, 303, 188
Knobel C. et al., 2009, ApJ, 697, 1842
Larson R. B., Tinsley B. M., Caldwell C. N., 1980, ApJ, 237, 692
Lemson G., the Virgo Consortium, 2006, preprint (astro-ph/0608019)
Mamon G. A., Biviano A., Murante G., 2010, A&A, 520, A30
Mamon G. A., Biviano A., Boué G., 2013, MNRAS, 429, 3079
Marinoni C., Davis M., Newman J. A., Coil A. L., 2002, ApJ, 580, 122
Martínez V. J., Saar E., 2002, Statistics of the Galaxy Distribution. Chapman & Hall, CRC [chapter 7.8]
Mauduit J.-C., Mamon G. A., 2007, A&A, 475, 169
Merchán M., Zandivarez A., 2002, MNRAS, 335, 216
Moore B., Frenk C. S., White S. D. M., 1993, MNRAS, 261, 827
Muñoz-Cuartas J. C., Müller V., 2012, MNRAS, 423, 1583
Navarro J. F., Frenk C. S., White S. D. M., 1996, ApJ, 462, 563
Nolthenius R., White S. D. M., 1987, MNRAS, 225, 505
Old L. et al., 2014, MNRAS, submitted
Peng Y.-j. et al., 2010, ApJ, 721, 193
Planck Collaboration et al., 2013, A&A, preprint (arXiv:1303.5076)
Ramella M., Geller M. J., Huchra J. P., 1989, ApJ, 344, 57
Robotham A. S. G. et al., 2011, MNRAS, 416, 2640
Roukema B. F., Quinn P. J., Peterson B. A., Rocca-Volmerange B., 1997, MNRAS, 292, 835
Tago E., Saar E., Tempel E., Einasto J., Einasto M., Nurmi P., Heinämäki P., 2010, A&A, 514, A102
Tarjan R. E., van Leeuwen J., 1984, J. Assoc. Comput. Mach., 31, 245
Tempel E. et al., 2014, A&A, preprint (arXiv:1402.1350)
Trasarti-Battistoni R., 1998, A&AS, 130, 341
Turner E. L., Gott J. R., III, 1976, ApJS, 32, 409
von der Linden A., Wild V., Kauffmann G., White S. D. M., Weinmann S., 2010, MNRAS, 404, 1231
Wang L., Steinhardt P. J., 1998, ApJ, 508, 483
Yang X., Mo H. J., van den Bosch F. C., 2003, MNRAS, 339, 1057
Yang X., Mo H. J., van den Bosch F. C., Jing Y. P., 2005, MNRAS, 356, 1293
Yang X., Mo H. J., van den Bosch F. C., Pasquali A., Li C., Barden M., 2007, ApJ, 671, 153
Zandivarez A., Díaz-Giménez E., Mendes de Oliveira C., Ascaso B., Benítez N., Dupke R., Sodré L., Irwin J., 2014, A&A, 561, A71

APPENDIX A: GALAXY SEARCH

Implementing galaxy grouping algorithms, such as FoF, requires the search for galaxy neighbours, which can be very time consuming if one computes all $N(N-1)/2$ separations between the N galaxies. We proceed in two steps, first selecting galaxies meeting the transverse link, then restricting these galaxies to those that also meet the LOS link. We built a two-dimensional grid on the sky coordinates with constant steps in declination and steps proportional to $1/\cos\delta$ in right ascension so that the length in right ascension (at the mean declination of the band of cells) is roughly equal to the step in declination. For each galaxy, we determine the cells that require searching for neighbours, and then we search using spherical trigonometry relations (see an illustration of this method in Fig. A1). The LOS link is then checked (without subdividing into LOS cells).

The computer time required to build the FoF groups is substantially reduced compared to the brute-force computation between pairs. The bottleneck of our tests in;volves the computation of the harmonic mean radius when measuring the EG mass by the virial theorem (equation 17).

APPENDIX B: FRACTION OF FLAGGED GROUPS

Fig. B1 displays the fraction of flagged groups, either because their parent groups were split in the simulation box transformations
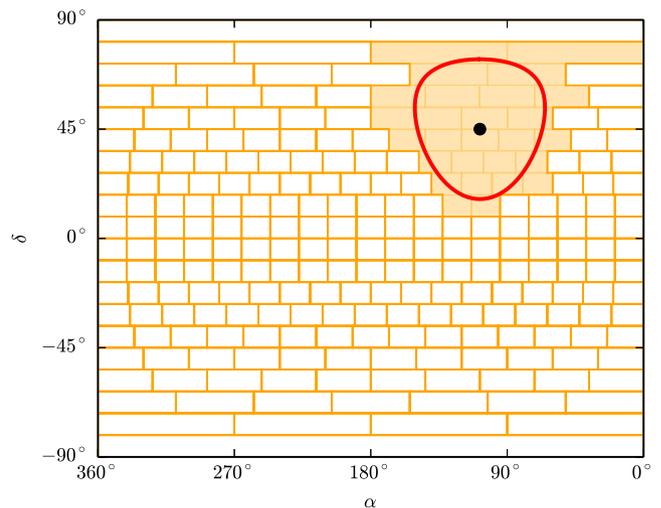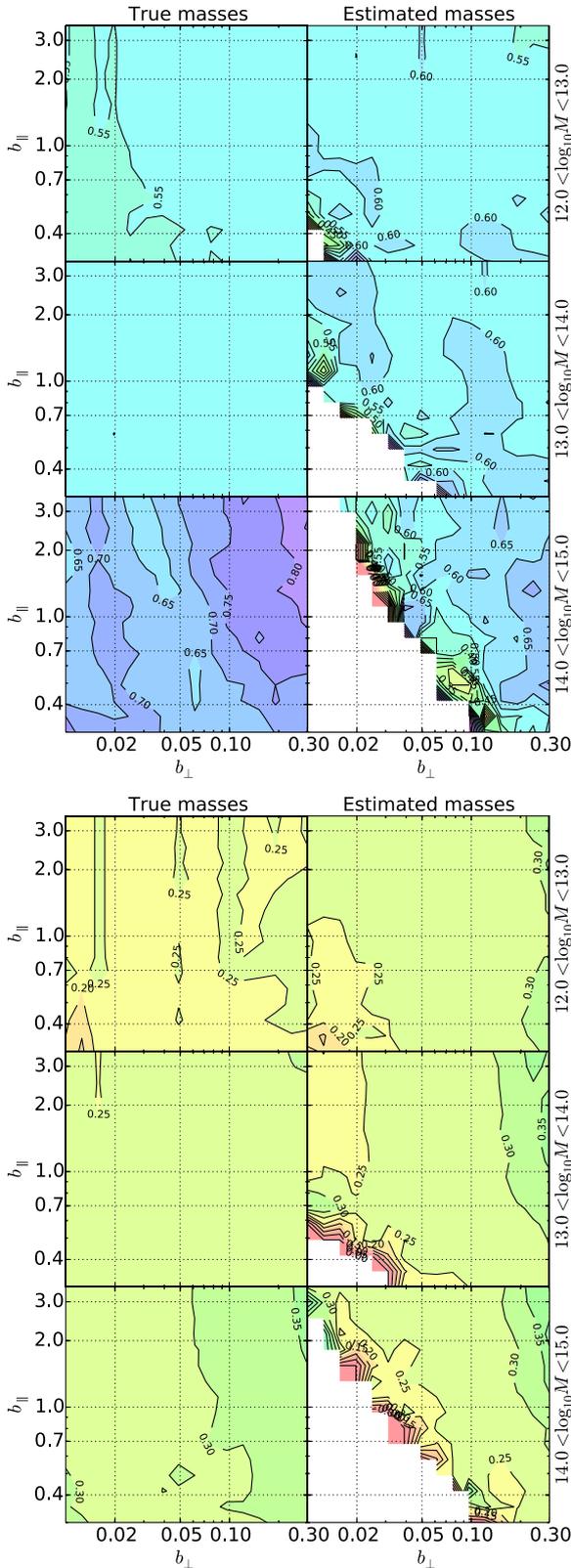

Figure A1. An illustration of the grid on the celestial sphere for a fast search of neighbours. Selected boxes to search are highlighted, for the given angular distance from the central point (red line). Note that both the search angle and the cell size are greatly exaggerated for illustrative purposes.

(Section 3) or because they are close to the survey edges and redshift limits. The fractions of flagged galaxies are greater in the nearby samples, because the survey edges and redshift limits are more important in this smaller volume sample.

Figure B1. Fraction of selected groups flagged as either split by the transformations of the simulation box or lying close to the edges of the mock galaxy survey for catalogues 2 (top) and 6 (bottom), in bins of true and estimated masses.

This paper has been typeset from a TEX/LATEX file prepared by the author.